metals

MDPI

Article

New FeMoTaTiZr High-Entropy Alloy for Medical Applications

Miguel López-Ríos [1], Julia Mirza-Rosca [1,2,*], Ileana Mariana Mates [3], Victor Geanta [4] and Ionelia Voiculescu [5]

[1] Mechanical Engineering Department, University of Las Palmas de Gran Canaria, 35001 Las Palmas de Gran Canaria, Spain
[2] Materials Engineering and Welding Department, Transilvania University of Brasov, 500036 Brasov, Romania
[3] Central Military Hospital Carol Davila, Calea Plevnei 134, 010242 Bucharest, Romania
[4] Faculty of Materials and Science Engineering, Politehnica University of Bucharest, 060042 Bucharest, Romania
[5] Faculty of Industrial Engineering and Robotics, Politehnica University of Bucharest, 060042 Bucharest, Romania
* Correspondence: julia.mirza@ulpgc.es

Abstract: High-entropy alloys are novel metallic materials distinguished by very special mechanical and chemical properties that are superior to classical alloys, attracting high global interest for the study and development thereof for different applications. This work presents the creation and characterisation of an FeMoTaTiZr high-entropy alloy composed of chemical constituents with relatively low biotoxicity for human use, suitable for medical tools such as surgical scissors, blades, or other cutting tools. The alloy microstructure is dendritic in an as-cast state. The chemical composition of the FeMoTaTiZr alloy micro-zone revealed that the dendrites especially contain Mo and Ta, while the inter-dendritic matrix contains a mixture of Ti, Fe, and Zr. The structural characterisation of the alloy, carried out via X-ray diffraction, shows that the main phases formed in the FeMoTaTiZr matrix are fcc $(Ti_7Zr_3)_{0.2}$ and hcp Ti_2Fe after annealing at 900 °C for 2 h, followed by water quenching. After a second heat treatment performed at 900 °C for 15 h in an argon atmosphere followed by argon flow quenching, the homogeneity of the alloy was improved, and a new compound like $Fe_{3.2}Mo_{2.1}$, $Mo_{0.93}Zr_{0.07}$, and $Zr(MoO_4)_2$ appeared. The microhardness increased over 6% after this heat treatment, from 694 to 800 $HV_{0.5}$, but after the second annealing and quenching, the hardness decreased to 730 $HV_{0.5}$. Additionally, a Lactate Dehydrogenase (LDH) cytotoxicity assay was performed. Mesenchymal stem cells proliferated on the new FeMoTaTiZr alloy to a confluence of 80–90% within 10 days of analysis in wells where the cells were cultured on and in the presence of the alloy. When using normal human fibroblasts (NHF), both in wells with cells cultured on metal alloys and in those without alloys, an increase in LDH activity was observed. Therefore, it can be considered that certain cytolysis phenomena (cytotoxicity) occurred because of the more intense proliferation of this cell line due to the overcrowding of the culture surface with cells.

Keywords: high-entropy alloys; chemical composition; microstructure; microhardness

Academic Editors: Chao Yang and Jiro Kitagawa

Received: 8 January 2025
Revised: 22 February 2025
Accepted: 26 February 2025
Published: 27 February 2025

Citation: López-Ríos, M.; Mirza-Rosca, J.; Mates, I.M.; Geanta, V.; Voiculescu, I. New FeMoTaTiZr High-Entropy Alloy for Medical Applications. *Metals* **2025**, *15*, 259. https://doi.org/10.3390/met15030259

1. Introduction

High-entropy alloys (HEA) are currently widely studied and developed due to their special mechanical and chemical properties, sometimes highly superior to those of conventional alloys [1–5]. Alloys containing chemical elements with extremely low toxicity have recently been obtained and tested for use in medical applications [6–8]. A wide variety of chemical compositions can be designed through combinations of highly corrosion-resistant and non-toxic elements to obtain concentrated solid solutions or high-entropy alloys from alloying systems such as W-Nb-Mo-Ta and W-Nb-Mo-Ta-V. Furthermore, another research

direction is focused on obtaining HEAs with a BCC structure, consisting of combinations between transitional metallic elements such as Nb-Mo-Ta-W, V-Nb-Mo-Ta-W, Ta-Nb-Hf-Zr-Ti, Hf-Nb-Ti-Mo-Ta-Ti-Zr, or the equiatomic alloy Hf-Mo-Nb-Ta-Ti-Zr. Such high-entropy alloys feature high yield strength (σ_y = 900–1600 MPa) at ambient temperature, as well as significant compressive strength [9]. Except for vanadium, most of the chemicals used to make these alloys are biocompatible. These alloys have recently been studied in the medical field for the manufacture of orthopedic implants (hip, knee, and shoulder prostheses), tending to replace pure titanium alloys or other alloys like Co-Cr-Mo alloys and stainless steels [10,11].

The stability of the solid BCC or FCC solutions in HEA alloys can be predicted by the valence electron concentration (VEC) values [12–14]. This stability is important for predicting the evolution of mechanical characteristics during successive decontamination stages at high temperatures. As high-entropy alloys (HEAs) are metallic compounds characterised by significant chemical heterogeneity arising from the combination of elements with substantial disparities in atomic diameters and diverse mutual solubility, the performance of heat treatments after alloy preparation was a solution used by most researchers in the field to achieve homogeneous matrices [15,16].

Chemical elements considered to have low toxic effects were added to the composition of the new alloy [17–19]. In some studies, Fe is considered a biocompatible element [20], but for a high concentration of iron in the blood, several unpleasant biochemical effects can occur, such as damage to DNA, proteins, lipids, or other cellular compounds [21]. In the long term, exposure to Fe-ions can even cause death. Titanium and zirconium alloys exhibit the highest biocompatibility of all metals in the body. Also, some alloys like Ti–Ta and Ti–Zr are used in dentistry due to their high wear resistance [21].

Heat treatments of high-entropy alloys can yield either hardening effects or enhanced flexibility and toughness, depending on the heating parameters and cooling methods employed [16,22–24]. Annealing for homogenisation can mitigate or eradicate the segregation consequences of chemical components that arise during the casting of high-entropy alloys [25,26]. This results in microstructures closer to equilibrium, either by dissolving the metastable phases or by the nucleation of the equilibrium phases, the formation of which was suppressed during rapid cooling. The result of annealing can also be the reduction of microscopic or macroscopic residual stress levels [21,26].

After solution treatment, the ultimate tensile strength of Ti–8Fe–8Ta–4Zr and Ti–10Fe–10Ta–4Zr alloys increased by 6% to 10% (1051 and 1092 MPa), this improvement being larger than those obtained after heat treatments of conventional biomedical titanium alloys such as Ti–6Al–4V ELI [27].

Regarding matrix hardening, in the case of high-entropy alloys, the main explanation is based on the precipitation hardening effects and the transition from FCC to the BCC + B2 hard phase. If the hard phase formed in the alloy is brittle, then the maximum strength reached is lower [28–31]. Even if they are intended for medical applications that do not involve long-term maintenance with biological tissue, such alloys must also be tested to highlight their biocompatibility and corrosion resistance [32].

This study presents some aspects regarding the attainment and characterisation of a new FeMoTaTiZr high-entropy alloy that can be used for non-implantable medical applications. The objective of this study was to obtain a strong enough alloy that can be used for medical instruments, such as surgical scissors, blades, or other cutting tools. The experimental alloy, obtained by melting high-purity raw materials, was microstructurally characterised to highlight the different types of phases and the distribution of chemical components inside the dendritic constituents. The measurement of the microhardness before and after performing of heat treatment showed that the homogenised metal matrix

strengthens after heat procedures between 3 and 6%, depending on the heating period and cooling media.

Cytotoxicity tests were performed by determining LDH (Lactate dehydrogenase) activity in human cells. The results accredited the idea that several bio ceramic coating layers must be cladded to improve the biocompatibility of the alloy. The pH values were between 7.6 and 7.7, similar in simple media, media incubated with alloys and media incubated with alloys and human fibroblasts. In media incubated with alloys and mesenchymal stem cells, moderately alkaline pHs of 7.8–7.9 were found, which normally favour the proliferation and osteogenic differentiation of these cells.

2. Materials and Methods

2.1. Material Preparation

The FeMoTaTiZr experimental alloy consisted of chemicals with extremely low biotoxicity for the human body, so it could be used for non-implantable medical devices. The experimental high-entropy alloys were obtained in the MRF ABJ 900 vacuum arc melting furnace (Allenstown, NH, USA) of the ERAMET-SIM-UPB Laboratory. For the experimental alloys, there were high-purity (over 99.5 wt.%) raw materials (metal elements), which were cleaned in an ultrasonic tank, in ethanol solution, before being introduced into the melting furnace. The metallic materials were weighed and dosed in equiatomic ratios for the composition of the alloy recipe, each batch weighing about 40 g.

Each micro-ingot was obtained via electric arc melting in an inert argon environment. For a molar mass of 472 g/mol, the design of chemical composition of the FeMoTaTiZr equiatomic alloy was as follows (wt.%): Fe = 11.88, Mo = 20.34, Ta = 38.34, Ti = 10.17, and Zr = 19.27, corresponding to the preliminary analysis of the local chemical composition performed using an EDAX Z2e sensor provided on the SEM Inspect S-FEI microscope (FEI Co., Eindhoven, The Netherlands), in wt.%: Fe = 12.46, Mo = 20.05, Ta = 36.25, Ti = 11.27, and Zr = 19.97. To obtain the melting conditions, the air in the installation was removed by blowing argon and successive vacuuming until a pressure of 5×10^{-3} mbar was obtained in the working chamber. The actual melting was performed in an argon environment at a pressure of 1.2 bar by slowly moving the electric arc along the load between the tungsten electrode and the metal batch. The melting operations were performed on each side of the mini-ingots, rotating them 8–10 times by 180°, to ensure the homogenisation and uniform distribution of the elements in the alloys.

After the successive melting operations, the batches were cooled under an argon atmosphere in the wells of the forced water-cooled copper plate. Within the experimental program, 6 batches were obtained, which were used for heat treatments as well as mechanical and microstructural characterisation.

The HEA mini ingots were weighed to calculate the efficiency of the production process used to assess the level of losses by vaporisation, oxidation, or projection in the form of drops in the electric arc. The small losses that were recorded after weighing the experimental alloys (between 0.1 and 0.3 g) showed the efficiency and good repeatability of the melting process. Each sample has dimensions of 9 mm × 15 mm × 60 mm (Figure 1).

2.2. Chemical Composition

Due to their high hardness (over 690 $HV_{0.5}$), the cast FeMoTaTiZr alloy samples used for morphological and structural characterisation were cut by spark electro-erosion. In order not to alter the values of the chemical composition, the samples were not etched with chemical reagents. The chemical composition of the experimental alloys determined on the central area of the sample using a SEM microscope (Hitachi TM3030Plus, Hitachi, Tokyo, Japan) equipped with energy dispersive spectrometry (EDS, Bruker, Germany).

The phase composition of the coatings was determined through X-ray diffraction (XRD) utilising CuKα radiation (SmartLab, Rigaku, Houten, The Netherlands) over a range of 20° to 80° with a step size of 0.02°/min. The values of the chemical composition were in good agreement with those calculated, because of the correct preparation, weighing, and melting procedure.

(**a**) (**b**)

Figure 1. (**a**) The metallic load placed on the copper plate of the VAR equipment and (**b**) FeMoTaTiZr mini-ingots of high-entropy alloy obtained by melting in RAV.

2.3. Microstructural Characterisation

Preliminary operations were performed on the samples, embedding them in epoxy resin, sanding afterwards with abrasive paper (360 to 2500 grain size), and polishing with alpha alumina abrasive paste (grain size between 0.3 and 0.01 µm) using Struers TegraPol-11 polishing equipment (Copenhagen, Denmark). These metallographic preparation techniques complied with ASTM E3-11 (2017) [33]. The Kroll reactive solution was employed for etching to analyse the surface of the sample. The OLYMPUS PME 3-ADL microscope (OlympusCorp., Tokyo, Japan) was subsequently employed for observations.

The morphological and structural characterisation was performed using the Auriga FESEM-FIB field emission scanning electron microscope (Carl Zeiss SMT, Oberkochen, Germany), with Gemini column for electron beam. The analysis involved X-ray diffraction conducted with the D8 Discover diffractometer (Bruker, Ettlingen, Germany). The setup included primary optics featuring a copper radiation tube (λ = 1.540598 Å) and a Göebel mirror (Bruker, Ettlingen, Germany), along with secondary optics equipped with a 1D LynxEye detector (Bruker, Ettlingen, Germany).

2.4. Heat Treatments and Microhardness

The heat treatments were performed using a Nabertherm LT 15/12/P320 furnace (Bremen, Germany) equipped with an automate regulator to maintain the parameters of the treatment. The micro-hardness was measured using the Shimadzu HMV 2T automatic tester (Shimadzu, Kyoto, Japan). In-line measurements were performed, spaced at about 1000 µm, on the homogenised zones of the ingots, before and after performing the heat treatments.

Based on the literature documentation on the effects of heat treatments performed on complex alloys with high Fe, Mo, Ta, Ti, and Zr content, it was found that the treatment temperature applicable to the FeMoTaTiZr multicomponent alloys should be in the range 900–1150 °C [29,31]. The chosen temperature for annealing was of 900 °C. The complete heat treatment procedure included the following sequence: annealing at 900 °C for 2 h in a Nabertherm furnace, followed by water quenching. The heating time was 65 min, the holding time within the maximum temperature range was 90 min, and the cooling time was 5 s. Finally, additional annealing was applied. The sample was heat-treated for 15 h in a controlled atmosphere (argon) at a temperature of 900 °C, followed by rapid cooling via argon flow purging.

2.5. Lactate Dehydrogenase (LDH) Cytotoxicity Assay

The cells used to evaluate the biocompatibility of the alloys were human bone mesenchymal stem cells (hBMSCs) isolated in the laboratory of the University of Tg. Mures (Targu Mures, Romania) and a cell line of normal human fibroblasts (NHF). Culture medium (cleared by centrifugation before testing) was analysed in duplicate for lactate dehydrogenase using the Cobas Integra 400 Plus biochemical analyzer (Roche Diagnostics, Barcelona, Spain). The activity of lactate dehydrogenase (LDH) was assessed using the UV enzymatic technique, which is frequently employed to evaluate cytotoxicity by detecting the activity of cytoplasmic enzymes released from compromised cells.

Cells in close contact with the HEA samples were examined using a Leica DMi8 (Leica Microsistemas SLU, L´Hospitalet de Llobregat, Spain) inverted microscope, employing filter cubes for FITC and Rhodamine fluorescence, followed by incubation with Calcein AM and Propidium Iodide. The study was conducted according to the ISO 10993 standard [34].

3. Results and Discussion

3.1. Microstructure

The alloy recipe was developed based on the equimolar participation of the constituent elements, considering that the elements should have atomic percentages as close as possible in the metal matrix. Mixing entropy for 5-element alloy over 1.5R, where R is the molar gas constant, is one of the values used to define the alloy as high-entropy alloy. The second-generation HEAs mainly refer to a class of HEAs containing more than four main elements and having a multiphase structure. Also, bulk metallic glasses or intermetallic compounds can be obtained from high-entropy combinations of elements. The δ-ΔH_{mix} Criteria and Ω Criteria serve as essential indicators for predicting solid solution formation [35]. Additionally, the effect of the alloy valence electron concentration is considered when evaluating the stability of the solid solution. The bond between the components will become disordered when the concentration of valence electrons fluctuates or surpasses a particular threshold, which reduces the stability of the solid solution and is beneficial for the creation of intermetallic compounds. These characteristics provide insight into atomic interactions, structural stability, and possible mechanical properties of the FeMoTaTiZr high-entropy alloy. To fully understand the way it functions, thorough experimental data (e.g., X-ray diffraction and mechanical testing) are frequently necessary.

As stated above, the design of chemical composition of the FeMoTaTiZr alloy in wt.% is Fe = 11.88; Mo = 20.34; Ta = 38.34; Ti = 10.17; Zr = 19.27, and the corresponding atomic concentrations are (at%): Fe = 20.06; Mo = 19.99; Ta = 19.98; Ti = 20.04; Zr = 19.92.

Theses atomic percentages will be used in the following calculations.

Mixing entropy ΔS_{conf} is obtained with the following formula:

$$\Delta S_{conf} = -\mathrm{R}\sum_{i=1}^{n} c_i ln c_i \quad (1)$$

where R is the gas constant, and c_i is the atomic ratio of the *i*-th element. Then, the calculated value is 1.609R, which is greater than 1.5R.

The δ parameter quantifies the atomic size discrepancy among the constituent elements in a high-entropy alloy. A bigger difference in atomic radii results in a larger δ value, which might affect the development of solid solutions or the long-term stability of the alloy.

The formula for δ parameter is

$$\delta = 100\sqrt{\sum_{i=1}^{n} c_i\left(1-\frac{r_i}{r_0}\right)^2} \quad (2)$$

where c_i and r_i are the atomic ratio and atomic radius of the component i, and r_0 is the weighted average of the atomic radii of all elements in the alloy. The atomic size of an element is affected by the surrounding atoms. The most useful radii for discussing metallic alloys are probably those for a coordination number of 12. Atomic radii used for the calculation are [36,37]: 127.4 pm (Fe), 140 pm (Mo), 146.7 pm (Ta), 146.2 pm (Ti), and 160.2 pm (Zr), resulting in the value r_0 = 145.89 pm. Then, the calculated delta parameter value is $\delta \approx 7.4\%$.

The formula for the mixing enthalpy (ΔH_{mix}) is

$$\Delta H_{mix} = \sum_{\substack{i=1 \\ i \neq j}}^{n} c_i c_j 4 \Delta H_{mix}^{AB} \quad (3)$$

where c_i and c_j are the atomic ratio of components i and j, respectively; r_0 is the weighted average of the atomic radii of all elements in the alloy; and ΔH_{mix}^{AB} is the mixing enthalpy of the binary alloy consisting of the i-th and j-th component in regular solution obtained through Miedema model. Mixing enthalpy values are shown in Table 1 [38]. Then, the calculated mixing enthalpy parameter value is $\Delta H_{mix} = -11.1$ kJ/mol.

Table 1. Values of the mixing enthalpy (kJ/mol) of the binary alloy for FeMoTaTiZr system.

Binary Alloy	Mixing Enthalpy (kJ/mol)
Fe-Mo	−2.0
Fe-Ta	−15.0
Fe-Ti	−16.8
Fe-Zr	−24.6
Mo-Ta	−4.9
Mo-Ti	−3.6
Mo-Zr	−6.2
Ta-Ti	1.4
Ta-Zr	2.7
Ti-Zr	−0.2

It can be found that solid solution phase formation is fixed for an atomic radius difference under 6.6% and when the mixing enthalpy of the alloy is within a certain range ($-20 < \Delta H_{mix} < 5$ kJ/mol). Under these conditions, the solid solution phase of the multicomponent alloy is easily formed with respect to the amorphous phase and the intermetallic compound [35]. Following the diagram published by Zhang et al. [39] that relates δ to the mixing enthalpy of the as-cast multicomponent alloys, it can be seen that for the atomic radius difference obtained (δ = 7.4%) and the mixing enthalpy of −11.1 kJ/mol, the alloy is out of the solid solution phase formation range. For this point in the diagram, intermediate phase formation is expected.

More multicomponent alloy systems have been calculated by other scientists, and the resulting impact of mixing enthalpy on phase stability was illustrated by Guo et al. [40], where solid solutions can develop when δ is small ($\delta < 6.6\%$) and ΔH_{mix} is either slightly positive or negligibly negative ($-11.6 < \Delta H_{mix} < 3.2$ kJ/mol); the formation of the amorphous phase is almost exactly contrary to these requirements when δ is large ($\delta > 6.4\%$) and ΔH_{mix} is noticeably negative ($\Delta H_{mix} < -12.2$ kJ/mol). Then, intermetallic compounds can develop under intermediate conditions regarding δ and ΔH_{mix}.

So, for the FeMoTaTiZr samples, δ-ΔH_{mix} criteria are not fulfilled because of the δ value being slightly over the limit. Following this analysis line, a single-phase solid solution may not be obtained, but intermediate phases and intermetallic compounds can.

The Ω Criterion is presented to take into account the influence of the thermodynamic stability of configurational entropy (ΔS_{mix}). It is calculated using the following formula:

$$\Omega = \frac{T_m \Delta S_{mix}}{|\Delta H_{mix}|} \tag{4}$$

where ΔS_{mix} is the configurational entropy, and T_m is the weighted average of the components melting point. The mixing enthalpy opposes the formation of a solid solution, whereas $T_m \Delta S_{mix}$ is favourable to its formation. Thus, values of $\Omega > 1$ may determine the formation of solid solution [35].

ΔS_{mix} can be obtained with the following formula:

$$\Delta S_{mix} = \Delta S_{conf} = -R \sum_{i=1}^{n} c_i \ln c_i \tag{5}$$

where R is the molar gas constant.

A value of Ω = 2.9 is obtained, which creates the possibility of solid solution formation.

For multicomponent high-entropy alloys, the VEC of the alloy is obtained with the following formula:

$$\mathrm{VEC} = \sum_{\mathrm{i}=1}^{\mathrm{n}} \mathrm{c_i VEC_i} \tag{6}$$

where $(\mathrm{VEC})_\mathrm{i}$ and $\mathrm{c_i}$ are the VEC and the atomic ratio for the *i*-th element, respectively.

The following $(\mathrm{VEC})_\mathrm{i}$ values were used [41]: 8 (Fe), 6 (Mo), 5 (Ta), 4 (Ti), and 4 (Zr). Then, the calculated value of the valence electron concentration for the alloy is 5.40. The stability of FCC and BCC solid solutions in high-entropy alloys was investigated by Guo et al. from Hong Kong Polytechnic University in relation to the valence electron concentration (VEC) [42]. The FCC solid solution phase is thought to be stable when VEC $\geq$ 8.6, whereas the BCC solid solution phase is thought to be relatively stable when VEC < 6.87. However, it cannot be used as a criterion for the formation of a high-entropy alloy phase; rather, it can only be used to determine which structure of the solid solution in the high-entropy alloy is easier to form [41].

Figure 2 displays optical images of the sample, before and after annealing at 900 °C for 2 h in furnace atmosphere, showing both a dendritically structure. Figure 2b shows the oxidation effects located preferentially on the interdendritic area (black mini area) that were produced by keeping the heated alloy in an unprotected atmosphere. For this reason, another annealing was performed in a controlled atmosphere (argon) at the same temperature but with a longer holding period (15 h). This time, cooling was performed in an argon flow medium (Figure 3). SEM images of samples after annealing at the same temperature but for different maintanance times are presented in Figure 3a (2 h, in furnace atmosphere) and Figure 3b (15 h in argon atmosphere).

Analing the SEM images of a cross-section through the ingot (Figure 3), it was observed that the appearance of the dendrites was modified after the second annealing, and they became rounded. Also, the oxidation effects were reduced, resulting in better alloy homogeneity. The semi-quantitative composition spectra of the zone integrated with elemental mapping for the central zone of the analysed alloy (Figure 3a) are presented in Figure 4, highlighting the composition of the alloy (wt.%): 26.9% Zr, 25.8% Ta, 17.9% Mo, 15.2% Fe, 13.1% Ti, and 1.1% Si. The distribution map of the elements providing indications regarding the constituents is shown in Figure 5. The presence of small amounts of oxygen

and Si (1.1 wt.%) probably comes from grit paper (SiC and Al_2O_3), being located mainly in dendrites, along with Mo and Ta. All chemical elements from the alloy are well distributed in the dendritic metallic matrix.

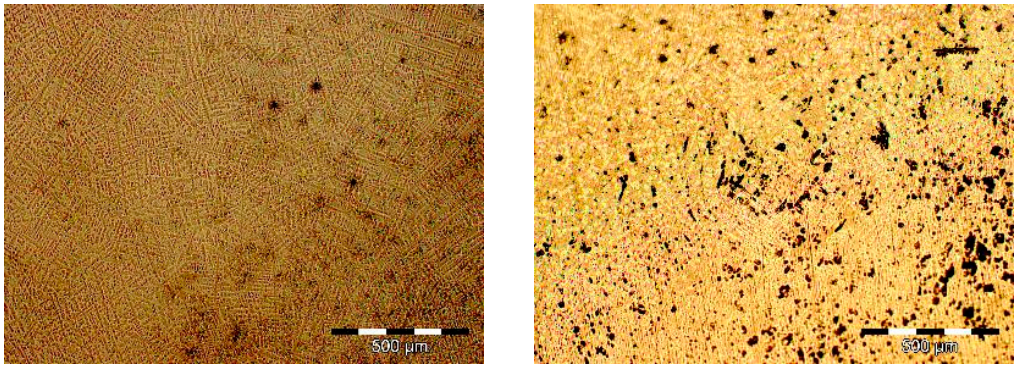

(**a**) (**b**)

Figure 2. Optical images of the the FeMoTaTiZr multicomponent alloy: (**a**) before first heat treatment and (**b**) after heat treatment.

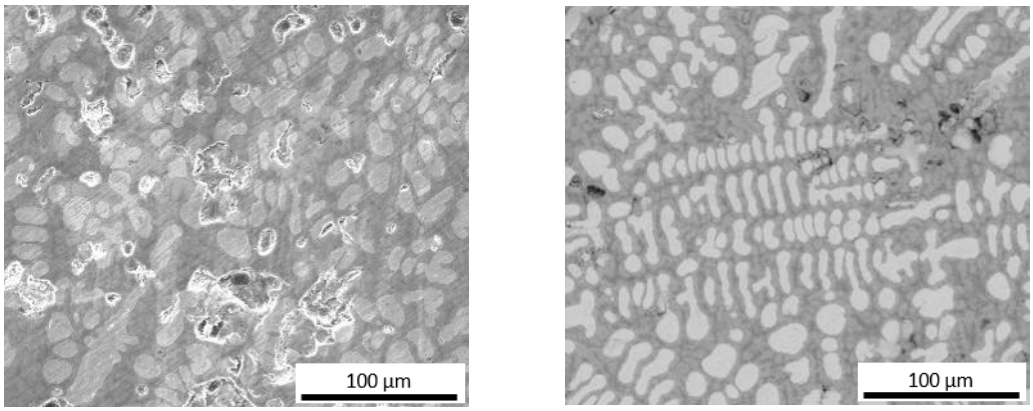

(**a**) (**b**)

Figure 3. SEM images of the FeMoTaTiZr multicomponent alloy: (**a**) after annealing at 900 °C for 2 h in furnace atmosphere; (**b**) after annealing at 900 °C for 15 h in argon atmosphere.

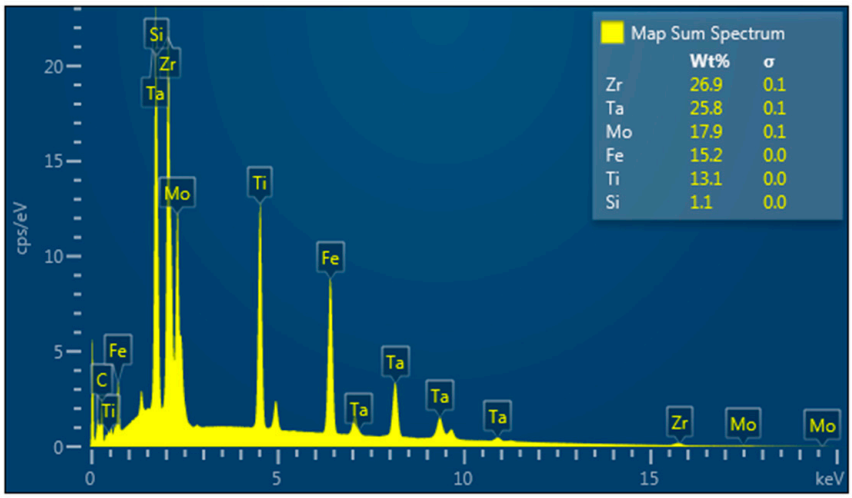

Figure 4. Semi-quantitative composition spectra of the area integrated with elemental mapping from Figure 3a.

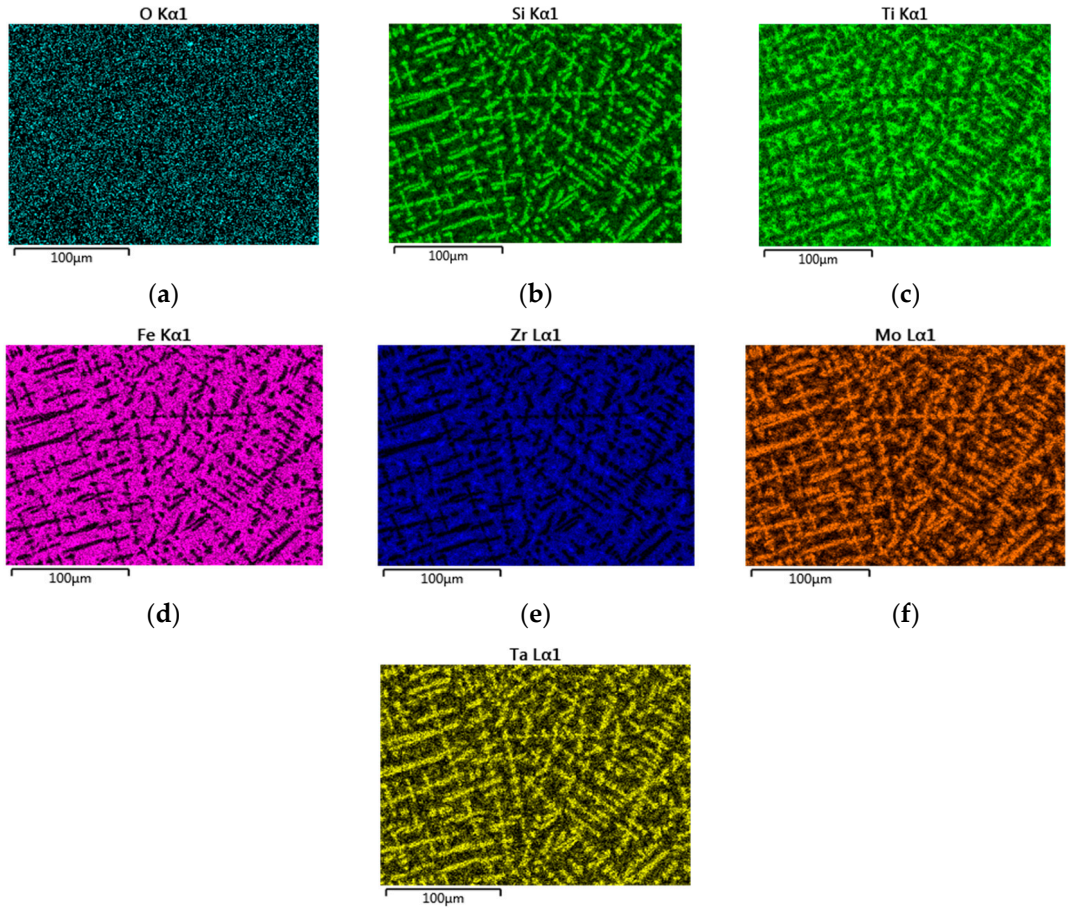

Figure 5. Map of the distribution of the elements in the microstructure of the FeMoTaTiZr alloy in the central region after casting: (**a**) O; (**b**) Si; (**c**) Ti; (**d**) Fe; (**e**) Zr; (**f**) Mo; (**g**) Ta.

The results yielded by the composition analysis were confirmed by X-ray diffraction tests. The diffraction patterns were captured with an angular increment of 0.040 at a scanning rate of 1 s per step. The qualitative analysis utilised the ICDD Release 2014 database. The X-ray diffraction diagram of the FeMoTaTiZr multicomponent alloy is shown in Figure 6.

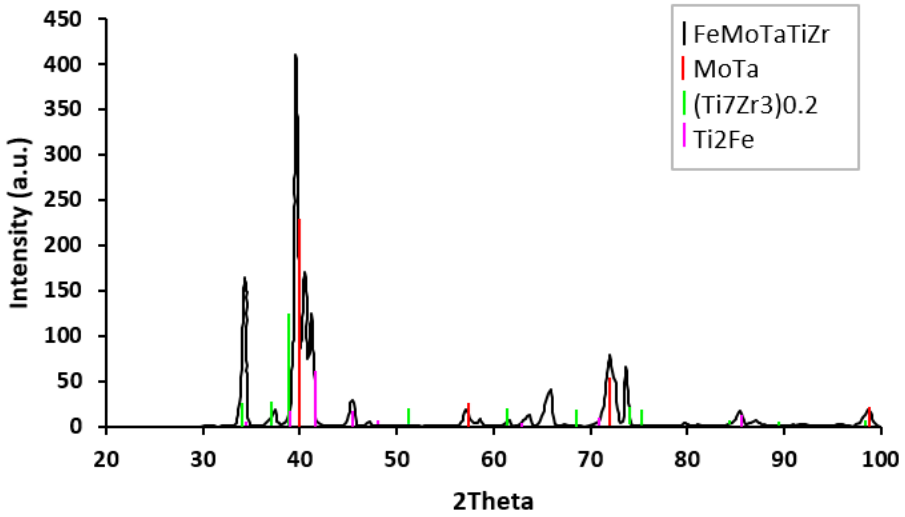

Figure 6. X-ray diffraction diagram of the as-cast FeMoTaTiZr multicomponent alloy.

The indications of the diagram in Figure 6 indicate the presence of the following constituents: bcc MoTa, hcp $(Ti_7Zr_3)_{0.2}$, fcc Ti_2Fe, and bcc Mo. The MoTa compound features the clearest indication (maximum peak), located at an angle of 2θ~40°. The presence validates the findings derived from mapping associated with the composition of dendrites in the FeMoTaTiZr high-entropy alloy. The other two constituents, $(Ti_7Zr_3)_{0.2}$ at an angle 2θ = 34° and Ti_2Fe at an angle 2θ = 41.5°, progressively separate from the metal melt at different temperatures, according to the mutual solubility and the electrochemical affinity of the constituent elements, contributing to the composition of the dendritic matrix.

To homogenise the solid solution, a first heat treatment (annealing followed by quenching) was performed. After the annealing, the homogeneity of the alloy was improved, the mass proportions of the constituents identified in the alloy being relatively close, but differences were found in terms of the constituents identified in the alloy in the cast state and those identified in the heat-treated state (Figure 7).

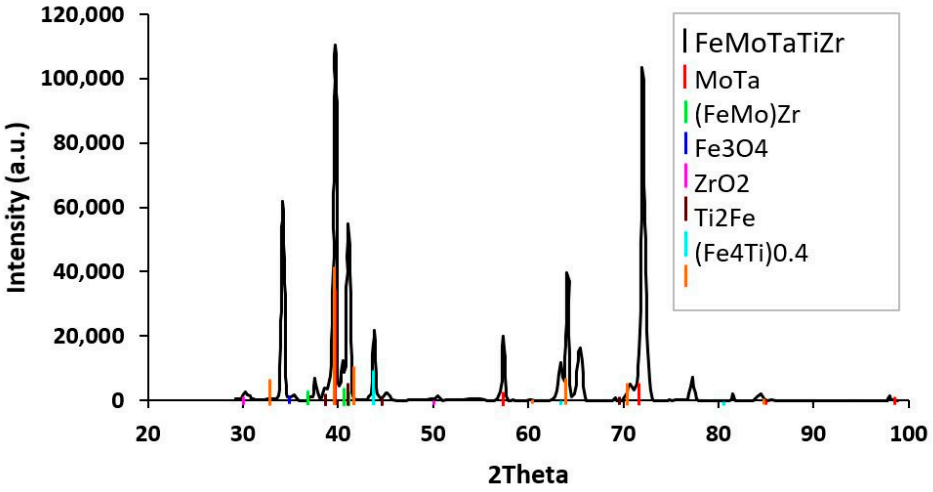

Figure 7. X-ray diffraction spectrum of FeMoTaTiZr alloy sample heat-treated in air at 900 °C/2 h, followed by fast cooling in water.

Some constituents, like oxides such as ZrO and Fe_3O_4, appeared in the solid solution due to the heat treatment conditions (heating in furnace atmosphere without protection, followed by cooling in water). Other compounds, such as $Fe_{0.2}Mo_{1.8}Zr$ and $(Fe_4Ti)_{0.4}$, are also present. The real changes brought to the alloy by heat treatment were obtained by annealing for 15 h in a controlled atmosphere (argon) at a temperature of 900 °C, followed by rapid cooling by argon flow purging.

In the analysis of the constituents identified (Figure 8), the long-period heat treatment led to the disappearance of the solid phase (FeMo)Zr and the appearance of new compounds, $Fe_{3.2}Mo_{2.1}$, $Mo_{0.93}Zr_{0.07}$, and $Zr(MoO_4)_2$. Also, the compounds based on Ti and Fe were modified, and instead of Ti_2Fe and Ti_7Zr_3, the compounds $Ti_{0.801}Fe_{0.197}$ and TiZr, respectively, appear. This is the consequence of maintaining for longer periods of time at high temperatures, when it is possible to separate some compounds from the initial solid solution matrix [31]. An additional microstructure study of the samples after a second annealing was conducted. A SEM image of the annealed area is shown in Figure 9, keeping a clear dendritic structure in which the tendency for dendrites to round is observed. Semi-quantitative composition spectra of different regions of the SEM image are shown in Figure 10.

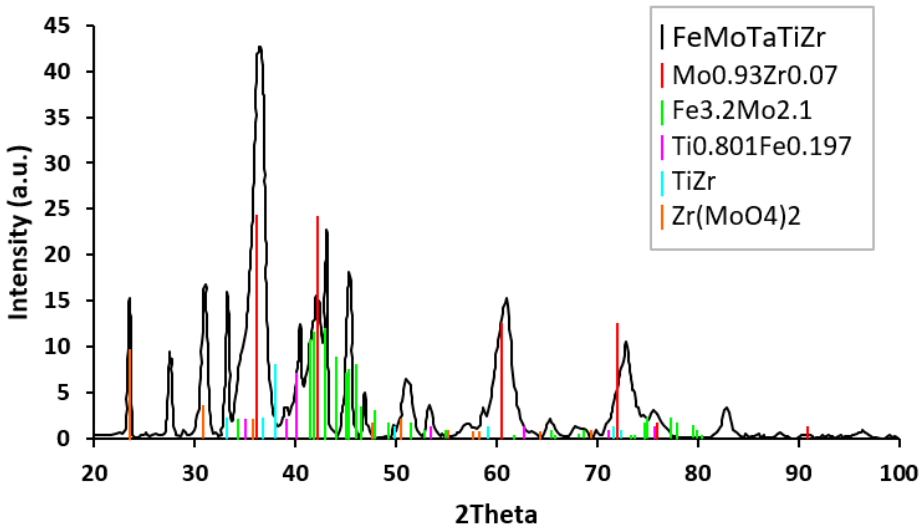

Figure 8. XRD results for FeMoTaTiZr alloy heat treated at 900 °C for 15 h in argon atmosphere followed by fast cooling in argon flow. The black and red lines represent the observed and calculated intensities in comparison.

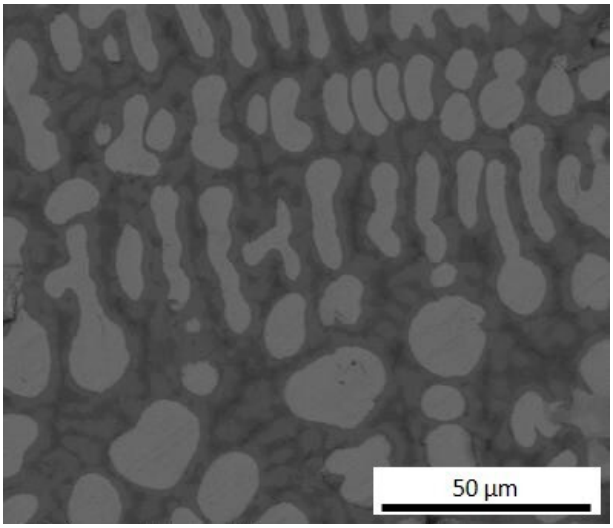

Figure 9. SEM micrograph of the FeMoTaTiZr alloy after annealing at 900 °C for 15 h.

In the semi-quantitative composition spectra (Figure 10), the dendrites in the annealed micro-areas are homogeneous from a compositional point of view. The chemical composition depends on the measurement area. Figure 10a shows the composition inside the dendrite, whereas Figure 10b–d shows the composition in the interdendritic regions. The chemical composition of the dendrites (Figure 10a) in the analysed micro area is within quite narrow limits, as follows (wt.%): Ta: 50.7–53, Mo: 36.8–38.2, Ti: 5.7–6.2, Zr: 2.4–2.6, and Fe: 1.3–1.7, and the oxygen content is constant, O: 0.9. These values clearly indicate that the dendrites are preferentially composed of chemical elements such as Ta and Mo, while in the interdendritic areas, the main elements are Zr, Fe, and Ti. The elements in the interdendritic region of the alloy had compositions within the following value ranges (wt.%): Zr: 33.8–37.8, Fe: 20.5–25.6, Ti: 15.1–19.7, Ta: 10.2–17.5, Mo: 5.6–11.9. Also, in this region, the oxygen content is constant at O: 1.2.

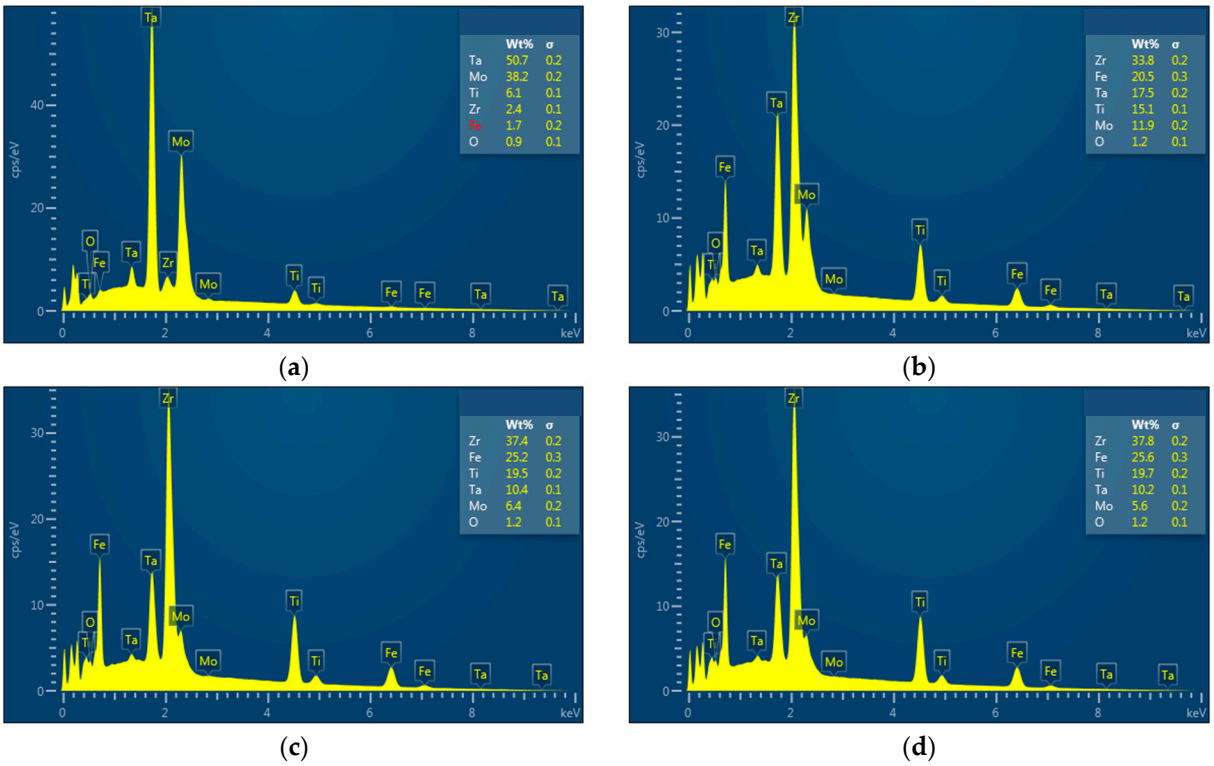

Figure 10. Image of secondary electrons and semi-quantitative composition of FeMoTaTiZr alloy after heat treatment at 900 °C for 15 h: (**a**) dendritic region and (**b**–**d**) interdendritic region.

3.2. Microhardness

The hardness was measured on both cast and heat-treated alloys, and the measurement values are shown in Table 2. The hardness measurements were performed in the homogenised zones of the ingots, on the cross-sections, using 10 different indentations, with a test force of 4.903 N and a load time of 10 s. The average hardness of the FeMoTaTiZr alloy in the cast state was 694 $HV_{0.5}$, and the heat treatment hardened it to 800 $HV_{0.5}$. The hardening level in the case of this alloy is more than 6% higher than the value obtained in the cast state.

Table 2. Microhardness values for FeMoTaTiZr samples in different thermal processing stages.

Alloy	Individual Values					Average Value	Variation Coefficient
As-cast (without heat treatment)							
FeMoTaTiZr	701	696	693	700	679	694	1.28
After annealing at 900 °C for 2 h							
FeMoTaTiZr	739	784	901	767	811	800	7.75
After annealing at 900 °C for 15 h							
FeMoTaTiZr	720	725	743	732	735	731	3.1

The considerable differences between the hardness values can be attributed to the presence of hard phases distributed in different zones of the metallic matrix. After performing the second annealing at 900 °C for 15 h, the microhardness decreased to 731 $HV_{0.5}$ due to stress relief effects; the dissolution of the solid phase (FeMo)Zr; and the appearance of new compounds like $Fe_{3.2}Mo_{2.1}$, $Mo_{0.93}Zr_{0.07}$, and $Zr(MoO_4)_2$.

3.3. Lactate Dehydrogenase (LDH) Cytotoxicity Assay

Lactate dehydrogenase (LDH) is an inert cytoplasmic enzyme present in all cells. LDH is swiftly released into the culture media when the plasma membrane of cultured cells is compromised during apoptosis, necrosis, and other types of cellular injury. The culture conditions provided enough cells (5–6 $\times$ 10^6 cells) for characterising cell viability and proliferation on the metallic substrate. Mesenchymal stem cells harvested from a 75 cm^2 tube were counted, checked for viability, and sub-cultured into two 75 cm^2 tubes (split ratio 1:2). The cells used to evaluate the biocompatibility of the alloys were human bone mesenchymal stem cells isolated in laboratory and a normal human fibroblast (NHF) cell line, kindly provided by Professor Mark Slevin from the Angiogenesis and Vascular Biology group at Manchester Metropolitan University.

Cells were stained with a Live/Dead Cell Double Staining Kit (Sigma cat. No. D4511-1KT-F) containing fluorochromes Propidium Iodide (PI) and Calcein AM. The optimal concentration established was 5 µL of PI and 10 µL of Calcein AM in 10 mL of phosphate-buffered saline (PBS) solution. Cytotoxicity was assessed by evaluating the activity of cytoplasmic enzymes produced from injured hBMSCs (human bone mesenchymal cells) and NHFs (normal human fibroblast cells). The degree of cell proliferation, viability, and adhesion of cells upon contact with the experimental alloy was monitored. The epifluorescence microscopy technique shows that cells have adhered to the alloy surface, making it necessary to investigate the adhesion and cellular morphology with specific markers in confocal microscopy. Using the same technique, cellular proliferation was observed both in the proximity of the alloy and on its surface. Cells in direct contact with the alloy samples were analysed in the Leica DMi8 inverted microscope using FITC and Rhodamine fluorescence cubes after incubation with Calcein AM and Propidium Iodide. The phase contrast image was also acquired on the same microscopic field of view (FOV), which allows for easy visualisation of the alloy sample in the well. For comparison, the evolution of the biological material prepared in the well without the presence of the metallic alloy was analysed after 5 and 10 days (Figure 11).

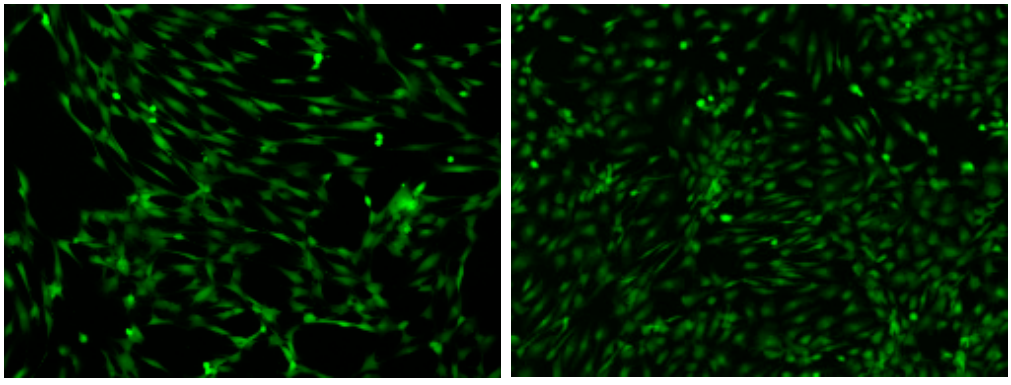

(**a**) (**b**)

Figure 11. Viability, adhesion, and proliferation of mesenchymal stem cells isolated from bone tissue in control wells, without alloy (fluorescence 100×): (**a**) after 5 days; (**b**) after 10 days.

At the same time, wells in which biological solutions were cultivated on discs taken from metal alloys were also examined after the same maintenance periods (Figure 12).

The phase contrast image was also acquired on the same microscopic field of view (FOV), which allowed for easy visualisation of the alloy sample in the well (Figure 13).

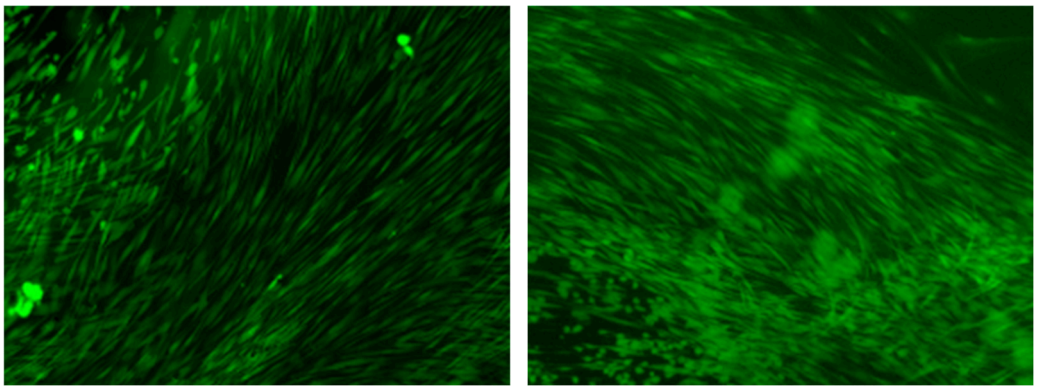

(**a**) (**b**)

Figure 12. Viability, adhesion, and proliferation of mesenchymal stem cells isolated from bone tissue in control wells with alloy (fluorescence 100×): (**a**) after 5 days; (**b**) after 10 days.

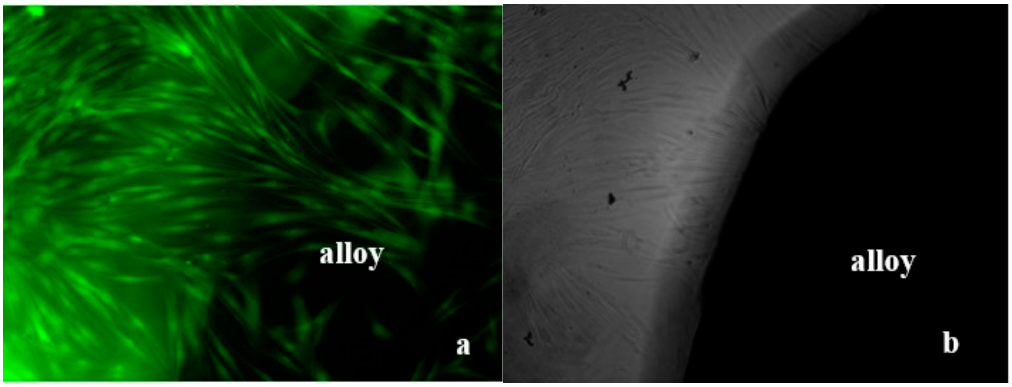

Figure 13. Viability, adhesion, and proliferation of human fibroblast cell line upon contact with FeMoTaTiZr alloys after 10 days. (**a**) Fluorescence, 100×; (**b**) phase contrast in same observation field, 100×.

In the images presented in Figures 11–13, it is observed that cellular proliferation from 80 to 90% confluence of the human fibroblast line was obtained both in the vicinity of the alloy and on its surface. In cytotoxicity tests performed on FeMoTaTiZr alloys, increases in LDH activity were recorded after 10 days in culture, with values double those in control wells with NHF and values 3.7 times higher than those in control wells with hBMSC.

The increase in LDH activity occurred both in the wells with cells cultured on alloys and in the wells with cells cultured without alloys, which means that it was not the presence of the metal alloy disc that led to certain cytolysis phenomena (cytotoxicity). At the same time, it was found that the greatest increases in LDH activity were recorded in the wells in which NHF were cultured. They have a higher proliferation capacity and cause overcrowding of the cell culture surface, causing the occurrence of apoptosis and necrosis in cell cultures.

4. Conclusions

The FeMoTaTiZr high-entropy alloy consisted of chemicals with low bio-toxicity for the human body, which occurs in classic alloys used in the manufacturing of non-implantable medical devices. The EDS analysis indicated a good agreement between the values of the chemical compositions proposed and obtained for the experimental alloys.

Values of mixing enthalpy and mixing entropy are in line with the formation of a solid solution, but the atomic size discrepancy among the constituent elements is slightly out

of range, which is not favourable for solid solution formation. Multi-phase solid solution formation is more likely to happen.

The morphological characterisation of the cast FeMoTaTiZr alloys highlighted a predominantly dendritic structure. The compositional analysis performed using the dispersive energy probe and the structural characterisation of the alloy, performed using X-ray diffraction, revealed the dendritic separation of the MoTa-type compounds in the fine dendritic matrix composed of $(Ti_7Zr_3)_{0.2}$ and Ti_2Fe-type constituents.

Annealing at 900 °C for 2 h performed in a furnace without a protective atmosphere, followed by quenching in water, promoted a high oxidation effect located preferentially on the interdendritic area. On the contrary, annealing at 900 °C for 15 h performed in an inert atmosphere (argon) followed by cooling in continuous argon flow created a better effect of homogenisation of the microstructure; dissolution of some compounds initially separated from the solid solution, like (FeMo)Zr; stress relief of the matrix; and reduction of hardness; as well as the appearance of new compounds, such as $Fe_{3\cdot2}Mo_{2\cdot1}$, $Mo_{0\cdot93}Zr_{0\cdot07}$, and $Zr(MoO_4)_2$.

Microhardness tests performed on the FeMoTaTiZr alloy, both in the as-cast state and after combined annealing and quenching heat treatments, revealed changes in the hardening effects of the metallic matrix.

Thus, annealing at 900 °C with a 2 h hold time in a furnace without a controlled atmosphere, followed by quenching in water, resulted in an increase in hardness from 694 $HV_{0.5}$ to 800 $HV_{0.5}$, the hardening level being over 6%. Annealing at the same temperature and a 15 h hold time in an inert atmosphere, followed by cooling in an argon flow, created a reduction in hardness from 800 to 730 $HV_{0.5}$.

Following cell proliferation tests and observations made using optical and phase contrast microscopy, it was established that the FeMoTaTiZr alloy allowed cell adhesion and multiplication to 80 and 90% confluence after 5 and 10 days of maintenance, respectively. Cytotoxicity tests showed that there is a slight cytotoxic reaction towards hBMSCs more sensitive than NHF cells. This phenomenon of cytolysis (cytotoxicity) occurred due to the more intense proliferation of this cell line because of the overcrowding of the culture surface with cells. Observations on the proliferation level with an increased intensity of NHF solutions led to the idea that a lower density per well, of approximately 10–20 $\times$ 10^4, is necessary.

Author Contributions: M.L.-R.: investigation, methodology and conceptualisation, and writing of the original draft; I.M.M.: investigation and methodology; V.G.: investigation, methodology, and writing—review and editing; I.V.: investigation, methodology, and writing—review and editing; J.M.-R.: data validation, project administration, visualisation, and review and editing. All authors have read and agreed to the published version of the manuscript.

Funding: This research received no external funding.

Data Availability Statement: The original contributions presented in this study are included in the article. Further inquiries can be directed to the corresponding authors.

Acknowledgments: We hereby acknowledge the project "The Smart Healthcare Engineering (SHEng)", with number 2023-1-RO01-KA220-HED-000159985, co-funded by the European Union. We also acknowledge Mark Slevin from the Angiogenesis and Vascular Biology group at Manchester Metropolitan University (UK), as well as the Hajnal Kelemen and Doina Manu from the University of Tg. Mures (Romania) for their assistance and advice in the cytotoxicity investigation.

Conflicts of Interest: The authors declare no conflicts of interest.

References

1. George, E.P.; Curtin, W.A.; Tasan, C.C. High Entropy Alloys: A Focused Review of Mechanical Properties and Deformation Mechanisms. *Acta Mater.* **2020**, *188*, 435–474. [CrossRef]
2. Han, L.; Zhu, S.; Rao, Z.; Scheu, C.; Ponge, D.; Ludwig, A.; Zhang, H.; Gutfleisch, O.; Hahn, H.; Li, Z.; et al. Multifunctional High-Entropy Materials. *Nat. Rev. Mater.* **2024**, *9*, 846–865. [CrossRef]
3. Mishra, R.S.; Haridas, R.S.; Agrawal, P. High Entropy Alloys—Tunability of Deformation Mechanisms through Integration of Compositional and Microstructural Domains. *Mater. Sci. Eng. A* **2021**, *812*, 141085. [CrossRef]
4. Yeh, J.-W.; Chen, S.-K.; Lin, S.-J.; Gan, J.-Y.; Chin, T.-S.; Shun, T.; Tsau, C.-H.; Chang, S.Y. Nanostructured High-Entropy Alloys with Multiple Principal Elements: Novel Alloy Design Concepts and Outcomes. *Adv. Eng. Mater.* **2004**, *6*, 299–303. [CrossRef]
5. Brito-Garcia, S.; Jimenez-Marcos, C.; Mirza-Rosca, J.; Voiculescu, I. Behavior of Ti-doped CoCrFeMoNi High Entropy Alloy. *Microsc. Microanal.* **2023**, *29*, 439–444. [CrossRef]
6. Zhang, E.; Zhao, X.; Hu, J.; Wang, R.; Fu, S.; Qin, G. Antibacterial Metals and Alloys for Potential Biomedical Implants. *Bioact. Mater.* **2021**, *6*, 2569–2612. [CrossRef] [PubMed]
7. Bandyopadhyay, A.; Mitra, I.; Goodman, S.B.; Kumar, M.; Bose, S. Improving Biocompatibility for next Generation of Metallic Implants. *Prog. Mater. Sci.* **2023**, *133*, 101053. [CrossRef]
8. Baltatu, M.S.; Spataru, M.C.; Verestiuc, L.; Balan, V.; Solcan, C.; Sandu, A.V.; Geanta, V.; Voiculescu, I.; Vizureanu, P. Design, Synthesis, and Preliminary Evaluation for Ti-Mo-Zr-Ta-Si Alloys for Potential Implant Applications. *Materials* **2021**, *14*, 6806. [CrossRef]
9. Yang, W.; Pang, S.; Liu, Y.; Wang, Q.; Liaw, P.K.; Zhang, T. Design and Properties of Novel Ti–Zr–Hf–Nb–Ta High-Entropy Alloys for Biomedical Applications. *Intermet* **2022**, *141*, 107421. [CrossRef]
10. Wang, S.-P.; Xu, J. TiZrNbTaMo High-Entropy Alloy Designed for Orthopedic Implants: As-Cast Microstructure and Mechanical Properties. *Mater. Sci. Eng. C* **2016**, *73*, 80–89. [CrossRef] [PubMed]
11. Todai, M.; Nagase, T.; Hori, T.; Matsugaki, A.; Sekita, A.; Nakano, T. Novel TiNbTaZrMo High-Entropy Alloys for Metallic Biomaterials. *Scr. Mater.* **2017**, *129*, 65–68. [CrossRef]
12. Wang, J.; Bai, S.; Tang, Y.; Li, S.; Liu, X.; Jia, J.; Ye, Y.; Zhu, L. Effect of the Valence Electron Concentration on the Yield Strength of Ti–Zr–Nb–V High-Entropy Alloys. *J. Alloys Compd.* **2021**, *868*, 159190. [CrossRef]
13. Oh, M.C.; Lee, H.; Sharma, A.; Ahn, B. Controlled Valence Electron Concentration Approach to Tailor the Microstructure and Phase Stability of an Entropy-Enhanced AlCoCrFeNi Alloy. *Metall. Mater. Trans. A* **2022**, *53*, 1831–1844. [CrossRef]
14. Yang, S.; Liu, G.; Zhong, Y. Revisit the VEC Criterion in High Entropy Alloys (HEAs) with High-Throughput Ab Initio Calculations: A Case Study with Al-Co-Cr-Fe-Ni System. *J. Alloys Compd.* **2022**, *916*, 165477. [CrossRef]
15. Mirza-Rosca, J.; Hulka, I.; Fratila, A.; Saceleanu, A. Surface Characterization of 5M NaOH Ti-Ta Treated Alloys Exposed to Simulated Body Fluid. *Microsc. Microanal.* **2023**, *29*, 1259–1261. [CrossRef]
16. Malatji, N.; Lengopeng, T.; Pityana, S.; Popoola, A.P.I. Effect of Heat Treatment on the Microstructure, Microhardness, and Wear Characteristics of AlCrFeCuNi High-Entropy Alloy. *Int. J. Adv. Manuf. Technol.* **2020**, *111*, 2021–2029. [CrossRef]
17. Wang, W.; Yang, K.; Wang, Q.; Dai, P.; Fang, H.; Wu, F.; Guo, Q.; Liaw, P.K.; Hua, N. Novel Ti-Zr-Hf-Nb-Fe Refractory High-Entropy Alloys for Potential Biomedical Applications. *J. Alloys Compd.* **2022**, *906*, 164383. [CrossRef]
18. Surmeneva, M.; Grubova, I.; Glukhova, N.; Khrapov, D.; Koptyug, A.; Volkova, A.; Ivanov, Y.; Cotrut, C.M.; Vladescu, A.; Teresov, A.; et al. New Ti–35Nb–7Zr–5Ta Alloy Manufacturing by Electron Beam Melting for Medical Application Followed by High Current Pulsed Electron Beam Treatment. *Metals* **2021**, *11*, 1066. [CrossRef]
19. Matsuno, H.; Yokoyama, A.; Watari, F.; Uo, M.; Kawasaki, T. Biocompatibility and Osteogenesis of Refractory Metal Implants, Titanium, Hafnium, Niobium, Tantalum and Rhenium. *Biomaterials* **2001**, *22*, 1253–1262. [CrossRef] [PubMed]
20. Gąsior, G.; Szczepański, J.; Radtke, A. Biodegradable Iron-Based Materials—What Was Done and What More Can Be Done? *Materials* **2021**, *14*, 3381. [CrossRef]
21. Chen, Q.; Thouas, G.A. Metallic Implant Biomaterials. *Mater. Sci. Eng. R Rep.* **2015**, *87*, 1–57. [CrossRef]
22. Xiang, T.; Zhao, M.; Du, P.; Xie, G. Heat Treatment Effects on Microstructure and Mechanical Properties of TiZrNbTa High-Entropy Alloy. *J. Alloys Compd.* **2023**, *930*, 167408. [CrossRef]
23. Guo, W.; Li, J.; Qi, M.; Xu, Y.; Ezatpour, H.R. Effects of Heat Treatment on the Microstructure, Wear Behavior and Corrosion Resistance of AlCoCrFeNiSi High-Entropy Alloy. *Intermet* **2021**, *138*, 107324. [CrossRef]
24. Brito-Garcia, S.; Jimenez-Marcos, C.; Mirza-Rosca, J.; Voiculescu, I. An investigation of elastic modulus in Zr doped CoCrFeMoNi HEA by three-point bending. *Microsc. Microanal.* **2023**, *29*, 439–444. [CrossRef]
25. Schuh, B.; Völker, B.; Todt, J.; Schell, N.; Perrière, L.; Li, J.; Couzinié, J.P.; Hohenwarter, A. Thermodynamic Instability of a Nanocrystalline, Single-Phase TiZrNbHfTa Alloy and Its Impact on the Mechanical Properties. *Acta Mater.* **2018**, *142*, 201–212. [CrossRef]
26. Senkov, O.; Scott, J.; Senkova, S.; Meisenkothen, F.; Miracle, D.; Woodward, C. Microstructure and Elevated Temperature Properties of a Refractory TaNbHfZrTi Alloy. *J. Mater. Sci.* **2012**, *47*, 4062–4074. [CrossRef]

27. Kuroda, D.; Kawasaki, H.; Yamamoto, A.; Hiromoto, S.; Hanawa, T. Mechanical Properties and Microstructures of New Ti–Fe–Ta and Ti–Fe–Ta–Zr System Alloys. *Mater. Sci. Eng. C* **2005**, *25*, 312–320. [CrossRef]
28. Chang, Y.-J.; Jui, C.-Y.; Lee, W.-J.; Yeh, A.-C. Prediction of the Composition and Hardness of High-Entropy Alloys by Machine Learning. *JOM* **2019**, *71*, 3433–3442. [CrossRef]
29. Yao, H.; Qiao, J.-W.; Hawk, J.; Ma, S.; Zhou, H. MoNbTaV Medium-Entropy Alloy. *Entropy* **2016**, *18*, 189. [CrossRef]
30. Liang, S.; Wang, Y.; Li, Y.; Gong, J.; Wu, W.; Hu, L.; Chen, Z. Structure and Mechanical Properties of Ambient Ductile TiZrNbHf Refractory High-Entropy Alloy: A First Principles and Experimental Study. *Vacuum* **2025**, *233*, 113910. [CrossRef]
31. Sheikh, S.; Bijaksana, M.K.; Motallebzadeh, A.; Shafeie, S.; Lozinko, A.; Gan, L.; Tsao, T.-K.; Klement, U.; Canadinc, D.; Murakami, H.; et al. Accelerated Oxidation in Ductile Refractory High-Entropy Alloys. *Intermet* **2018**, *97*, 58–66. [CrossRef]
32. Gartland, A.; Rumney, R.M.; Dillon, J.P.; Gallagher, J.A. Isolation and Culture of Human Osteoblasts. In *Human Cell Culture Protocols*; Picot, J., Ed.; Humana Press: Totowa, NJ, USA, 2005; pp. 29–54, ISBN 978-1-59259-861-8.
33. *ASTM E3-11*; Standard Guide for Preparation of Metallographic Specimens. ASTM International: West Conshohocken, PA, USA, 2017.
34. *ISO 10993-5*; Biological Evaluation of Medical Devices. Part 5: Tests for in Vitro Cytotoxicity. Springer: Berlin/Heidelberg, Germany, 2009.
35. Zhang, Y. Microstructures and Properties of High Entropy Alloys. *Prog. Mater. Sci.* **2014**, *61*, 1–93. [CrossRef]
36. Teatum, E.; Gschneidner, K.J.; Waber, J. *Compilation of Calculated Data Useful in Predicting Metallurgical Behavior of the Elements in Binary Alloy Systems*; Los Alamos National Laboratory (LANL): Los Alamos, NM, USA, 1959.
37. Calvo-Dahlborg, M.; Brown, S.G.R. Hume-Rothery for HEA Classification and Self-Organizing Map for Phases and Properties Prediction. *J. Alloys Compd.* **2017**, *724*, 353–364. [CrossRef]
38. Takeuchi, A.; Inoue, A. Calculations of Mixing Enthalpy and Mismatch Entropy for Ternary Amorphous Alloys. *Mater. Trans. JIM* **2000**, *41*, 1372–1378. [CrossRef]
39. Zhang, Y.; Zhou, Y.; Lin, J.; Chen, G.; Liaw, P. Solid-Solution Phase Formation Rules for Multi-component Alloys. *Adv. Eng. Mater.* **2008**, *10*, 534–538. [CrossRef]
40. Guo, S.; Hu, Q.; Ng, C.; Liu, C.T. More than Entropy in High-Entropy Alloys: Forming Solid Solutions or Amorphous Phase. *Intermet* **2013**, *41*, 96–103. [CrossRef]
41. Guo, S.; LIU, C.T. Phase Stability in High Entropy Alloys: Formation of Solid-Solution Phase or Amorphous Phase. *Progress. Nat. Sci.-Mater. Int.* **2011**, *21*, 433–446. [CrossRef]
42. Guo, S.; Ng, C.; Lu, J.; Liu, C. Effect of Valence Electron Concentration on Stability of Fcc or Bcc Phase in High Entropy Alloys. *J. Appl. Phys.* **2011**, *109*, 3587228. [CrossRef]